https://doi.org/10.5194/angeo-2020-7
Preprint. Discussion started: 3 March 2020

Annales Geophysicae Discussions
Open Access
EGU

The VLF transmitters' radio wave anomalies related to 2010 Ms 7.1 Yushu earthquake observed by DEMETER satellite and the possible mechanism

Shufan Zhao[1*], XuHui Shen[1], Zeren Zhima[1] and Chen Zhou[2]

[1] Institute of Crustal Dynamics, China Earthquake Administration, Beijing 100085, China

[2] School of Electronic Information, Wuhan University, Wuhan, 430072, China

* Correspondence: zsf2008bj@126.com

Abstract: Earthquakes may disturb the lower ionosphere through various coupling mechanisms during their seismogenic and coseismic periods. The VLF signal radiated from ground-based transmitters will get affected when it penetrates the disturbed region in the ionosphere above the epicenter area, and this anomaly can be recorded by low earth orbit satellite under certain conditions. In this paper, the temporal and spatial variation of the Signal to Noise Ratio (SNR) of the VLF transmitter signal in the ionosphere over the epicenter of 2010 Yushu Ms 7.1 earthquake in China is analyzed. The results show that the SNR over the epicenter of Yushu earthquake especially in the southwestern region decreased (or dropped)revealed by one satellite revisit period before the main shock, which is consistent with the observed TEC anomaly at same time, implying that the decrease of SNR might be caused by the enhancement of TEC. A full-wave method was used to study the mechanism of the change of SNR before the earthquake. When the electron density in the lower ionosphere increases by four times, the electric field will decrease about 1 dB, indicating that the disturbed electric field decrease 20% compared with the original electric field and vice versa. It can be concluded that the variation of electron density before earthquakes may be one important factor influence the variation of SNR.

Keywords: 2010 Yushu earthquake, DEMETER satellite, VLF radio wave, signal to noise ratio, lower ionospheric disturbance, Full-wave model

1. Introduction

The VLF (Very Low Frequency) radio waves radiated by the powerful ground-based VLF transmitters have been utilizing for long distance communication and submarine navigation, because of the efficient reflection within the earth-ionosphere waveguide. However, there is still a small fraction of the wave energy can leak into the higher ionosphere and magnetosphere after being absorbed by the lower ionosphere. The signals from transmitters observed by the LEO (Low Earth Orbit) satellite can be used to research the propagation of VLF wave in the earth-ionosphere waveguide and ionosphere, as well as wave-particle interaction in the radiation belt (Cohen and Marshall, 2012; Inan et al., 2007; Inan and Helliwell, 1982; Lehtinen and Inan, 2009; Parrot et al., 2007).

It is gradually confirmed that earthquake abnormal precursors not only appear near the ground, but also may couple with the atmosphere and ionosphere through some mechanisms, resulting in plasma disturbances in the ionosphere and recorded by such as ionosonde and GPS-TEC (Global positioning system-Total electron

https://doi.org/10.5194/angeo-2020-7
Preprint. Discussion started: 3 March 2020

content) (Liu et al., 2009; Liu et al., 2001; Liu et al., 2006; Pulinets et al., 2000; Stangl et al., 2011; Zhao et al., 2008). Therefore, when the VLF radio waves propagate upward through the earthquake affecting ionospheric disturbance area, the VLF signals received by the ground VLF receivers and satellite will change, which have been recorded by (Hayakawa, 2007; Maurya et al., 2016; Molchanov et al., 2006; Píša et al., 2013). In these research, Molchanov et al. (2006) have applied the VLF data recorded by satellite to study the earthquake abnormality for the first time. They found the SNR (Signal to Noise Ratio) of the electric field from VLF transmitters recorded by DEMETER (Detection of Electro-Magnetic Emission Transmitted from Earthquake Regions) satellite decreased near the epicenters during a series of earthquakes. The larger the magnitude of the earthquake; the larger the spatial zone of SNR reduction is. However, it is hard to distinguish the coseismic anomaly and precursory anomaly from their results.

Two devastating earthquakes, the 2008 Ms 8.0 Wenchuan earthquake and the 2010 Ms 7.1 Yushu earthquake, have occurred successively in southwestern China during the operation period (2004-2010) of DEMETER satellite. Some research also focused on the SNR variation of VLF transmitters using DEMETER satellite observation to extract the earthquake related anomalies before the two strong earthquakes (He et al., 2009; Shen et al., 2017; Yao et al., 2013). The results all illustrated the decrease of SNR before the earthquakes. Since the seismo-ionospheric disturbance zone does not uniformly appear above the epicenter, the location of the SNR abnormity in relation to the epicenter should be furtherly studied. Which factor influences the SNR and its possible mechanism, that is also needed to be comprehensively illustrated. Therefore, in this paper we investigate the temporal and spatial SNR variation of the VLF transmitter signal in the ionosphere over the epicenter of 2010 Ms 7.1 Yushu earthquake, as well as the background variation of SNR in the same period of 2007-2010 to be distinguished whether the SNR reduction is caused by earthquake events or just ionospheric background changes. The mechanism of how the seismo-ionospheric disturbance affect the variation of SNR has been discussed in this paper.

As the mechanism of the VLF radio wave variations in the altitude of LEO satellite (presented as SNR variation) before the earthquakes, Hayakawa (2007) and Píša et al. (2013) suggest the VLF anomalies exist because the lower ionosphere is lowered before earthquake. Molchanov et al. (2006) declared that the variation of SNR in the ionosphere is attributed to the plasma disturbance of the lower ionosphere. Furthermore, it has been found that the electron density variation only exists in the lower ionosphere according to the computer ionosphere tomography (CIT) results based on GPS-TEC data before Nepal Ms 8.1 earthquake in 2015 (Kong et al., 2018). The electric field penetrating model of Kuo et al. (2011) shown that the electron density variation in lower ionosphere can be induced by changes of the current in the global electric circuit which is also the main factor making the lower ionosphere lowered. On the other hand, Marshall et al. (2010) construct a 3D finite difference time domain model to simulate the lightning electromagnetic pulse and its interaction with the lower ionosphere. All the reports mentioned above demonstrate that the earthquake and lightning can disturb the electron density in the lower ionosphere. Many other studies also have found the main loss of VLF wave power mainly occurs in the lower ionosphere when VLF radio waves penetrate into ionosphere through calculations based on absorption curve or full wave model (Cohen and Inan, 2012; Liao et al., 2017; Starks et al., 2008; Tao et al., 2010; Zhao et al., 2017; Zhao et al., 2015). In sum, the electron density variation in the lower ionosphere might be one main factor causing SNR anomaly. Based on these results, the full-wave calculation model was utilized to study the influence of the electron density disturbance of the lower ionosphere on the variation of VLF radio signals.

https://doi.org/10.5194/angeo-2020-7
Preprint. Discussion started: 3 March 2020

Annales Geophysicae Discussions
Open Access
EGU

In this paper, a brief description of the DEMETER data and full-wave method used in this study are presented in Section 2. The temporal and spatial variations of SNR over the epicenter have been investigated before 2010 Yushu earthquake with four years (2007-2010) observation; the full-wave model is used to simulate how the variation of electron density in the lower ionosphere affects the electric field SNR of VLF transmitter at the altitude of DEMETER are presented in Section 3. The discussion and conclusions of this research are presented in Section 4 and 5.

2. Materials and Methods

2.1. Earthquake, VLF Transmitters, and DEMETER data

At the local time 07:49:37.9 of April 14, 2010, a Ms 7.1 earthquake hit the Yushu city, Qinghai Province with epicenter is located in 33.2° N, 96.6° E with a 14 km depth at the Northeastern Tibetan plateau. The nearest VLF transmitter around the epicenter is located in the proximity of Novosibirsk (NOV, in short) which belongs to the Russian Alpha navigation system which consists of three transmitters. The other two transmitters named Krasnodar (KRA) and Khabarovsk (KHA) are far away from Yushu earthquake, so only the satellite data radiated from NOV have been used to analyze in this paper. The location of the transmitters and the epicenter of Yushu earthquake are marked by blue squares and black stars respectively in Figure 1. Three different frequency VLF radio signals (11.9/12.6/14.9 kHz) are radiated from these three transmitters, with a 0.4 s duration and a 3.6 s cycle.

The DEMETER satellite was launched on 29 June 2004 as a sun-synchronous orbit at the altitude of 710 km, then was changed to 660 km in December 2005 (Parrot et al., 2006), and the mission was ended in December 2010. The scientific objective of the DEMETER is to detect and characterize the electromagnetic signals associated with natural phenomena (such as earthquakes, volcanic eruptions, tsunamis) or anthropogenic activities. It operated in the region from invariant latitude -65° to 65°, with descending and ascending orbits crossing the equator at local time ~10:00 and ~22:00, respectively. DEMETER has a re-visit orbit period of about 14-days, which means the satellite returns to the over the same orbit trajectory after 13 days. The payloads include several electromagnetic sensors with two working mode: burst and survey. At ELF/VLF band, the intensive electromagnetic wave data over locations of particular interest were provided in the burst mode, and in the survey mode, electric and magnetic power spectral density (PSD) data every 2 s were provided with sampling frequency 40 kHz and spectral resolution 19.53 Hz.

According to the formula of Dobrovolsky et al. (1979), the preparation zone of the earthquake can reach $\rho=10^{0.43M}$, M represents the magnitude of the earthquake in the formula. Considering the limited extension of the Ms 7.1 Yushu earthquake, the preparation zone ρ can reach to 1020 km, we mainly focused on the region with radius 600 km above the epicenter to minimize the influence of other unknown disturbing sources. In this study, the night-time PSD data of electric field from the DEMETER's survey mode observations within the region of epicenter ±10° (black square in Figure 1) were extracted, and the data within 600 km circle (shown in Figure 3) over the epicenter was used to study the perturbations of the VLF radio waves from the Russia transmitters before and after the Yushu earthquake. The spectrum data of the 1st re-visit period (April 2 to14) before the earthquake within 600 km are averaged shown as Figure 2 for example. It is clear that the signals from many VLF transmitters can be distinguished. Due to the VLF radio signals at daytime is

https://doi.org/10.5194/angeo-2020-7
Preprint. Discussion started: 3 March 2020

Annales Geophysicae Discussions
Open Access
EGU

too small to cause obvious SNR variation compared with that in night-time, we did not use the day-time data in this study.

2.2. The method to calculate SNR

According to the method of Molchanov et al. (2006), the SNR of electric field was calculated as follows:

$$SNR = \frac{2A(f_0)}{A(f_+)+A(f_-)} \quad (1)$$

where $A(f_0)$ is the amplitude of electric field spectrum at the central frequency, and $A(f_\pm)$ are the spectrums at $f_\pm = f_0 \pm \Delta f$, where Δf is the chosen frequency band. As can be seen in Figure 2, the VLF radio signals radiated from ground based VLF transmitters has different transmitting frequency bands. For the three Russian VLF transmitters, the f_0 is set as three VLF radio waves frequency radiated from NOV transmitters: 11.9/12.6/14.9 kHz, and the Δf=300 Hz.

2.3. Full wave method

A full-wave method has been used to seek a solution of Maxwell equations for plane waves varying as e^{jwt} in a horizontally-stratified medium with fixed dielectric permittivity tensors $\hat{\varepsilon}$ and permeability μ in each layer. Considering the region of our interest is much smaller than the radius of the earth, we can neglect the earth's curvature in the model of this study. A Cartesian coordinate system is established with x, y in the horizontal plane and z vertical upward. The solution of the Maxwell equations is given in a form of a linear combination of plane waves $\sim e^{j(k_\perp \cdot r_\perp)}$, where $k_\perp$ is the horizontal component of the wave vector k which is conserved by Snell's law inside each layer, we have

$$\begin{cases} k \times E = \omega\mu_0 H \\ k \times H = -\omega\hat{\varepsilon}E \end{cases} \quad (2)$$

Where ω is the angular frequency, μ is the permeability of the medium ($\mu \equiv 1$ for non-magnetic medium), $\hat{\varepsilon} = \varepsilon_0(I + \hat{\chi})$ is dielectric tensor, and $\hat{\chi}$ is electric susceptibility tensor (Yeh and Liu, 1972). $\hat{\chi}$ is determined by the electron density and collision frequency in the ionosphere, as well as the geomagnetic field. In our simulation, the electron density is obtained from International Reference Ionosphere (IRI) model, and the electron collision frequency (denoted by ν) is calculated by the exponential decay law with the height (denoted by h) increasing $\nu = 1.8\times10^{11}e^{-0.15h}$. The parameters of geomagnetic field at the location of the VLF transmitter is calculated by International Geomagnetic Reference Field (IGRF) model.

Eliminating the z components from equation (2), the following elegant form of Maxwell equations are obtained:

https://doi.org/10.5194/angeo-2020-7
Preprint. Discussion started: 3 March 2020

Annales Geophysicae Discussions
Open Access
EGU

144 $$\frac{dV}{dz} = jk_0 \hat{T} \cdot V \quad (3)$$

145 Where $V = (E_\perp, Z_0 H_\perp)$, Z_0 is wave impedance, $\hat{T}$ is a 4×4 matrix:

146 $$\hat{T} = \begin{pmatrix} -\frac{k_x \varepsilon_{31}}{k_0 \varepsilon_{33}} & -\frac{k_x \varepsilon_{32}}{k_0 \varepsilon_{33}} & \frac{k_x k_y}{k_0^2 \varepsilon_{33}} & 1 - \frac{k_x^2}{k_0^2 \varepsilon_{33}} \\ -\frac{k_y \varepsilon_{31}}{k_0 \varepsilon_{33}} & -\frac{k_y \varepsilon_{32}}{k_0 \varepsilon_{33}} & -1 + \frac{k_y^2}{k_0^2 \varepsilon_{33}} & -\frac{k_x k_y}{k_0^2 \varepsilon_{33}} \\ -\varepsilon_{21} + \frac{\varepsilon_{23}\varepsilon_{31}}{\varepsilon_{33}} - \frac{k_x k_y}{k_0^2} & -\varepsilon_{22} + \frac{\varepsilon_{23}\varepsilon_{32}}{\varepsilon_{33}} + \frac{k_x^2}{k_0^2} & -\frac{k_y \varepsilon_{23}}{k_0 \varepsilon_{33}} & \frac{k_x \varepsilon_{23}}{k_0 \varepsilon_{33}} \\ \varepsilon_{11} - \frac{\varepsilon_{13}\varepsilon_{31}}{\varepsilon_{33}} - \frac{k_y^2}{k_0^2} & \varepsilon_{12} - \frac{\varepsilon_{13}\varepsilon_{32}}{\varepsilon_{33}} + \frac{k_x k_y}{k_0^2} & \frac{k_y \varepsilon_{13}}{k_0 \varepsilon_{33}} & -\frac{k_x \varepsilon_{13}}{k_0 \varepsilon_{33}} \end{pmatrix} \quad (4)$$

147 The electromagnetic field in each layer can be obtained in the k (wave vector) domain by solving equation (3)
148 recursively (Budden, 1985; Lehtinen and Inan, 2008). More details of full-wave method is described in
149 Lehtinen and Inan (2008).

150 **3. Results**

151 *3.1. VLF signal analysis from DEMETER satellite*

152 To calculate the SNR of electric field, Firstly, we collected the DEMETER's observations 5 re-visit
153 periods before and 1 re-visit period after the earthquake in 2010 to study the evolution of SNR above the
154 epicenter of Yushu earthquake. The data of the same period in 2007-2010 during non-earthquake time were
155 also extracted to build the background trend of SNR as a reference to confirm the anomaly occurred during
156 the earthquake. In the first period from April 2 to 14, there are two magnetic storms occurred on April 4-7 and
157 April 11-12 and, the Dst index are -84 nT, -69 nT and Kp index are 7 and 5.3, respectively. To exclude the
158 influence of geomagnetic storms, we only selected the data during Kp<3 and Dst > -30 nT. Secondly the
159 spatial range of SNR was determined according to the formula of Dobrovolsky et al. (1979). The SNR
160 distributions of three VLF radio signals are selected within a radius 600km above the region of epicenter, as
161 shown in Figure 3, where the black star represents the epicenter of Yushu earthquake.

162 It can be found that the 1st re-visit period (April 2-14) before the earthquake, the SNR of VLF waves at
163 three frequency (11.9, 12.6, 14.9 kHz) all decrease dramatically over the earthquake compared with other
164 revisit periods. Furthermore, to make sure whether the SNR abnormal is caused by ionospheric background
165 variation or not, we analyzed the SNR variation of the same period in 2007-2010 (background time). As
166 shown in Figure 3, there are some missing orbital data due to the magnetic storms from April 2 to 14 and the
167 SNR in some days like Mar 28 and February 20 are very small in all orbit, which was because the transmitter
168 is turned off on these days. We excluded these data in the examination of the change of SNR in Figure 4 and 5.
169 To avoid the impact on the result because of lacking data, the mean value of all the data in the black circle of
170 every period have been obtained to get the time sequence shown in Figure 4. The black dash line represents
171 the occurred date of the earthquake in Figure 4. The black and red lines represent the average values in 5
172 periods before the earthquake and 1 period after the earthquake inside the circle of radius 600 km above the
173 epicenter in 2010 and background time, respectively. The change trends of SNR in background time and 2010
174 are the same except in the 1st period before the earthquake. The average value of SNR decreases in 1st period

https://doi.org/10.5194/angeo-2020-7
Preprint. Discussion started: 3 March 2020

Annales Geophysicae Discussions

before the earthquake in 2010 which is different from it in background time especially in 11.9 kHz. It means the decrease of SNR in 2010 might be caused by Yushu earthquake.

Furthermore, we focus on the daily changes of SNR in a period before the earthquake, To detect abnormal signals of the SNR variations, a quartile-based process is performed (Liu et al., 2009). The median (M) of every successive 11 days of the SNR of the whole orbits has been calculated to check the deviation between the SNR of the 12th day and the computed median (M). The lower (first) quartile (denoted as LQ in short) and the upper (third) quartile (UQ in short) have been calculated to provide the information about the deviation. Based on the assumption of the normal distribution of the SNR with the mean (m) and standard deviation (σ), the expected value of M and LQ or UQ are equals to m and 1.34σ ((Liu et al., 2009) and reference therein). We set the lower boundary (LB in short), LB = M+2(M-LQ) and the upper boundary (UB in short), UB= M+2(UQ-M) to find the SNR anomalies with a stricter criterion. Thus, if an observed SNR on the 12th day is greater or smaller than its previous 11-day-based UB or LB, a positive or negative abnormal of SNR will be identified. Figure 5 shows the time series of SNR at 11.9, 12.6, 14.9 kHz respectively. The red, gray, and two black curves denote the observed SNR and associated median and upper/lower bound (UB/LB), respectively. Blue and green sign represent the upper and lower anomalous days identified by the computer routine, respectively. The LB and UB are constructed by the 1–11 previous days' moving median (M), lower quartile (LQ), and upper quartile (UQ). There are no circles on the red, gray, black lines in some days because the data have been excluded as mentioned above. As we can see in the figure 5, besides the lower anomalies appeared on April 13 (one day before Yushu earthquake, the occurred time of Yushu earthquake denoted by vertical dashed line in Figure 5) at all transmitting frequency, there are another three anomalies occurred on March 29, April 8,and April 10 respectively. Previous research (ndicate the earthquake precursory usually occurred within one week before earthquake, so the lower anomaly occurred on March 29 at 12.6 and 14.9 kHz may have nothing to do with Yushu earthquake.

We speculate that the anomalies of SNR may be related to the anomalies of electron density. To confirm our conjecture, we used GPS-TEC MAP data distributed by CODE (Center for Orbit Determination in Europe) to check out whether the Total electron content (TEC) showing similar anomalies. The resolution of TEC data from CODE is 5°×2.5°, We use 11 days' sliding mean value of every grid as background, then we can get a spatial distribution of background. Background ± 2×stand deviation is set as threshold (Upper bound and Lower bound) to determine whether there have anomalies, if intraday value exceed the threshold represents there have anomalies. We have reviewed the TEC anomalies of every day from April 2 to April 14 (which means the duration of sliding background is from March 22 to April 13). The TEC anomalies only occurred April 13, especially the anomalies are the most intensive at UT 6:00 which means only the SNR anomaly at April 13 is possible earthquake precursory, the other two anomalies at April 8 and 10 may be caused by other factors. The top panel of Figure 6 shows the TEC at 6:00 am UT on April 13 and the sliding mean of background (April 2-12), the bottom panel shows the abnormal region where the TEC value exceed threshold (background ± 2×stand deviation). As we can see that the TEC had abnormal enhancement on April 13 at southwestern region of epicenter. Similar to this, the SNR of orbit No. 030939-1 on April 13 also decreased in the southwestern direction in Figure 3. This phenomenon maybe illustrates the decrease of SNR caused by TEC enhancement. Furthermore, this TEC enhancement was probably caused by earthquake, because it shows

https://doi.org/10.5194/angeo-2020-7
Preprint. Discussion started: 3 March 2020


Annales Geophysicae Discussions

very intensive conjugate response. However, TEC anomalies caused by geomagnetic storm do not exhibit this kind of phenomenon generally(Zhao et al., 2008).

3.2. The possible mechanism of SNR variation revealed by full-wave simulation

In section 3.1, we analyzed the spatial and temporal characteristics of SNR during the five-revisit period before and one revisit period after the Yushu earthquake. It can be found that the SNR decreased significantly before the earthquake over the epicenter area of Yushu earthquake, especially in the southwestern direction. After excluding the influence of geomagnetic storms, we furtherly explored the possible mechanism of SNR abnormal variation in this section. As mentioned in the section 1, the electron density in the lower ionosphere can be disturbed through various mechanisms before earthquakes. The electron density before Nepal earthquake was obtained from computer ionosphere tomography method by using GPS data (Kong et al., 2018). The left column (Figure 7 of (Kong et al., 2018)) is the variation of electron density at the height of 150 km. It can be seen that after UT 6:20, the electron density in the southwest of the epicenter decreases significantly compared with that before 6:20, while the electron density in the northwest and southeast of the epicenter increases significantly compared with that before 6:20, and the range of variation reaches about 30%. However the electron density hardly change at the height of 450 km (see Figure 7 in (Kong et al., 2018)). Marshall et al. (2010) have shown that 60 horizontal discharge pulses of 7 V/m can cause 50% change of electron density in lower ionosphere, and 60 horizontal discharge pulses of 10 V/m can even cause 400% change of electron density. Based on these results, the full-wave model was used to simulate the changes of the electric field at satellite altitude excited by ground-based VLF transmitter caused by the enhancement or decrease of electron density in the lower ionosphere, so as to furtherly determine the change law of SNR.

The full wave method (FWM) (Lehtinen and Inan, 2009) was utilized to simulate the electric field between altitudes of 0 - 120 km induced by NOV transmitter which is the closest transmitter to epicenter of Yushu earthquake. A Cartesian coordinate system was established with x, y in the horizontal plane and z vertical upward.

We set a Gaussian shape perturbation at 110 km with 20 km bandwidth in the ionosphere. The magnitude of the perturbation was set as maximum 4 times both increase and decrease compared to the original electron density of nighttime (the average electron density above NOV transmitter during 20100402-20100414 at LT 22:00 calculated from IRI-2016 model). The perturbation patterns are shown in the Figure 7. The other parameters of geomagnetic field and ionosphere are obtained from existing models which have been introduced in section 2.3.

The electric filed only from ground surface to 120km have been calculated by full wave model, Because the electromagnetic wave at VLF band will propagate upward as whistler mode. The group velocities of the upward radiated whistler-mode are almost parallel, and these waves form a narrow collimated beam which does not have much lateral spread. The direction of group velocities is determined by refractive index surface. The refractive index surface of the upgoing whistler mode at 120km is shown in Figure 8. A ducted propagation is adopted at this L shell (Clilverd et al., 2008) and the VLF wave power is spread in accordance with the divergence of geomagnetic field lines with a linear reduction because the mode conversion (Lehtinen and Inan, 2009; Shao et al., 2012).

https://doi.org/10.5194/angeo-2020-7
Preprint. Discussion started: 3 March 2020


Annales Geophysicae Discussions
Open Access
EGU

The simulated results of electric field at 120 km height with different electron density along the magnetic meridian plane within 1000 km area around the transmitter NOV are shown in Figure 9a. It can be seen that the wave mode interference in the wave-guide has been mapped into the ionosphere in the electric field (Lehtinen and Inan, 2009), and the electric field increases when the electron density decreases, and vice versa (Figure 9a). Furthermore, the maximum value of the electric field varying with height is collected to study the influence of the electron disturbance.

In the nighttime, it can be seen that when the electron density increases by four times, the maximum electric field decreases about 1 dB at 120 km (see figure 9b). The variation is also 1 dB at DEMETER's altitude (660 km) because of the linear reductions (Lehtinen and Inan, 2009; Shao et al., 2012), which implies that the disturbed electric field decrease 20% compared with the original electric field (Figure 9b). In a short time interval as a few days before the earthquake, the background noise can be assumed stable, so the change of electric field can reflect the change of SNR. It can be concluded when the electron density increases by four times, the variation of SNR is 20%. The simulated results illustrate that the variation of electron density in the lower ionosphere before earthquake is one main factor of causing the abnormal the variation of SNR. The more precise SNR variation needs more observation and simulation in the future.

4. Discussion

4.1. The possible mechanism on how the earthquake induces the disturbance in the lower ionosphere

Which coupling mechanism is effective to induce electron density anomalies in the D/E layer by earthquakes is still an open question. Molchanov et al. (2006) declared the lower ionospheric disturbance is caused by acoustic gravity wave triggered by earthquakes. At present, the coupling mechanism of electric field proposed by Pulinets (2009) is widely accepted because it has been demonstrated by a series models (Kuo et al., 2011; Namgaladze et al., 2013; Zhou et al., 2017) and observations (Gousheva et al., 2006; Gousheva et al., 2008; Li et al., 2017). As for 2008 Wenchuan Ms 8.0 earthquake in China, Li et al. (2017) reported continuous observations about the anomalous electric field which lasted longer but weaker than the electric field induced by lightning during one month before Wenchuan earthquake. He suggests that the abnormal electric field might be caused by the seismogenic activity of Wenchuan earthquake. Xu et al. (2011) also found about 2 mV/m anomalous electric field in the F2 layer of ionosphere before the Wenchuan earthquake. Gousheva et al. (Gousheva et al., 2006; Gousheva et al., 2008) revealed a large number of anomalous electric fields before earthquakes using the Intercosmos satellite. In additional, it is demonstrated that the anomalous electric field induced by earthquake could change the electron density in the lower ionosphere by Kuo et al. (2011) and Zhou et al. (2017). Such as 2015 M 8.1Nepal earthquake, the electron density variation was well explained by the ground electric field coupling model established by Zhou et al. (2017).

4.2. The other factors may induce disturbance in the lower ionosphere

The lightning, geomagnetic storms and other natural sources may induce disturbance in the lower ionosphere (Marshall et al., 2010; Maurya et al., 2016; Peter et al., 2006; Zigman et al., 2007). As known, the intensive TEC change occurs during geomagnetic storms, and the change of TEC is affected intensively

https://doi.org/10.5194/angeo-2020-7
Preprint. Discussion started: 3 March 2020

during the main phase of the geomagnetic storm, gradually return to normal accompany with the recovery phase. To avoid the effect of geomagnetic storms, the data which kp > 3 and Dst < -30 nT were excluded in this research and the TEC anomaly detected in Figure 6 showed on one day after the recovery phase of geomagnetic storm (top panel of Figure 10). Furthermore, the change pattern of TEC is totally different from the one caused by earthquake, because the TEC anomalies caused by geomagnetic storm expand from high-latitudes to mid-latitudes due to thermospheric neutral winds, E×B convection and so on (Pokhotelov et al., 2008). From bottom panel of Figure 10, we can see the all the SNRs of whole orbit are large in April 5,6,7,11 during geomagnetic storm, especially at the higher latitude. However, SNR pattern in April 13 is totally different. In sum, The TEC anomaly on April 13 should be unconcerned with geomagnetic storm. The lightning flash is very rare in our research region (only 4 events from Feb 2010 to Apr 2010, which can be get from the search result of website (https://lightning.nsstc.nasa.gov/nlisib/nlissearch.pl?coords=?579,18)), so the effect of lightning could be ignored in this study.

5. Conclusions

In this paper, the SNR of electric field from the Russian VLF transmitter observed by DEMETER satellite was analyzed before and after 2010 Ms 7.1 Yushu earthquake. The VLF signals from Russian VLF transmitters can be clearly observed at frequency of 11.9, 12.6, 14.9 kHz over the epicenter from the electric field spectrum data. To determine whether the SNR variation is related to Yushu earthquake, the data in quiet space weather conditions (kp ≤3 and Dst ≥ -30 nT) have been selected during five satellite revisit periods before the earthquake and one revisit period after the earthquake. The result shows that the SNR decreased during one revisit period before Yushu earthquake in all case. Our analysis on SNR variation also shows that the SNR in April 13 is smaller than that in other days over the epicenter, and the decrease of SNR is the most intensive at the southwestern region when we divide the space over the epicenter of earthquake into four regions. These results are consistent with the TEC anomalies in Figure 6. In addition, we also analyzed the SNR changes over the epicenter in the same period from 2007-2010 as background map and found that the SNR changes trend of one revisit period before the earthquake relative to background time were contrary to those in 2010. The change trend of SNR decreased in 2010 but increased in background time in the 1st revisit period before the earthquake. The change trend of SNR is the same in other revisit period both in 2010 and background time. In sum, it can be concluded that the SNR over the epicenter of Yushu earthquake decreases abnormally in one satellite revisit period before the earthquake, especially in the southwestern region of the earthquake, which is consistent with the observed TEC anomaly before the earthquake. The decrease of SNR before the Yushu earthquake may be due to the enhancement of electron density.

The electron density in the lower ionosphere may change abnormally before earthquake through some coupling mechanisms. The full wave simulation result on NOV, which is the nearest transmitter next to Yushu earthquake, indicates that the electric field at the altitude of satellite will change when we add a disturbance on electron density in the lower ionosphere. That is to say that the SNR of electric field will also change when the background noise is considered to be invariable a few days before the earthquake. The simulated results show that the SNR of electric field will decrease with the increase of electron density in the lower ionosphere; the SNR will increase with the decrease of electron density in the lower ionosphere. It can be concluded that the variation of electron density before earthquakes may be one important factor influence the variation of SNR.

https://doi.org/10.5194/angeo-2020-7
Preprint. Discussion started: 3 March 2020

We will continually explore the law of SNR change and verify the mechanism we proposed with more seismic events, by utilizing the newly launched LEO electromagnetic satellite (China Seismo-Electromagnetic Satellite) (Shen et al., 2018; Zhao et al., 2019) in next work.

Data Availability

The DEMETER satellite data were provided by DEMETER scientific mission center (http://demeter.cnrs-orleans.fr). The GPS-TEC data were provided by CODE (Center for Orbit Determination in Europe) and can be downloaded from the website ftp://cddis.gsfc.nasa.gov/pub/gps/products/ionex.

Author Contributions: Conceptualization, S.Z.; Formal analysis, S.Z.; Investigation, S.Z.; Methodology, S.Z., R.Z., and X.S.; Resources, S.Z., X.S. and R.Z.; Supervision, S.Z.; Visualization, S.Z.; Writing-original draft, S.Z.; Writing-review & editing, S.Z., R.Z, .C.Z., and X.S..

Corresponding author

Correspondence to Shufan Zhao.

Competing interests

The authors declare that they have no competing interests.

Funding: This work is supported by the National Science Foundation of China (Grant No. 41704156, 41574139, 41874174), National Key R&D Program of China (Grant No. 2018YFC1503501), the Special Fund of the Institute of Earthquake Forecasting, China Earthquake Administration (Grant No: 2015IES010103,2018CSES0203)and the APSCO Earthquake Research Project Phase II.

Acknowledgements

We acknowledge the DEMETER scientific mission center for providing data of DEMETER satellite (http://demeter.cnrs-orleans.fr). The GPS-TEC data were provided by CODE (Center for Orbit Determination in Europe) and can be downloaded from the website ftp://cddis.gsfc.nasa.gov/pub/gps/products/ionex.

References

1. Budden, K., 1985. The Propagation Of Radio Waves: The Theory Of Radio Waves Of Low Power In The Ionosphere And Magnetosphere. Cambridge University Press, Cambridge, United Kingdom.
2. Clilverd, M. A., Rodger, C. J., Gamble, R., Meredith, N. P., Parrot, M., Berthelier, J. J., and Thomson, N. R.: Ground-based transmitter signals observed from space: Ducted or nonducted? Journal of Geophysical Research Atmospheres 113, A04211, 2008.
3. Cohen, M. B., and Inan, U. S.: Terrestrial VLF transmitter injection into the magnetosphere. J. Geophys. Res.: Space Phys 117, 2012.
4. Cohen, M. B., and Marshall, R.: ELF/VLF recordings during the 11 March 2011 Japanese Tohoku earthquake. Geophys. Res. Lett. 39, 2012.
5. Dobrovolsky, I. P., Zubkov, S. I., and Miachkin, V. I.: Estimation of the size of earthquake preparation zones. Pure Appl. Geophys. 117, 1025-1044, 1979.
6. Gousheva, M., Glavcheva, R., Danov, D., Angelov, P., Hristov, P., Kirov, B., and Georgieva, K.: Satellite monitoring of anomalous effects in the ionosphere probably related to strong earthquakes. Advances in Space Research 37, 660-665, 2006.

https://doi.org/10.5194/angeo-2020-7
Preprint. Discussion started: 3 March 2020

7. Gousheva, M., Glavcheva, R., Danov, D., Hristov, P., Kirov, B. B., and Georgieva, K.: Electric field and ion density anomalies in the mid latitude ionosphere: Possible connection with earthquakes? Advances In Space Research 42, 206-212, 2008.
8. Hayakawa, M.: VLF/LF Radio Sounding of Ionospheric Perturbations Associated with Earthquakes. Sensors 7, 1141-1158, 2007.
9. He, Y., Yang, D., Chen, H., Qian, J., Zhu, R., and Parrot, M.: SNR changes of VLF radio signals detected onboard the DEMETER satellite and their possible relationship to the Wenchuan earthquake. Science in China Series D-Earth Sciences (in Chinese) 39, 403-412, 2009.
10. Inan, U. S., Golkowski, M., Casey, M., Moore, R., Peter, W., Kulkarni, P., Kossey, P., Kennedy, E., Meth, S., and Smit, P.: Subionospheric VLF observations of transmitter-induced precipitation of inner radiation belt electrons. Geophys. Res. Lett. 34, L02106, 2007.
11. Inan, U. S., and Helliwell, R. A.: DE-1 observations of VLF transmitter signals and wave-particle interactions in the magnetosphere. Geophys. Res. Lett. 9, 917–920, 1982.
12. Kong, J., Yao, Y., Zhou, C., Liu, Y., Zhai, C., Wang, Z., and Liu, L.: Tridimensional reconstruction of the Co-Seismic Ionospheric Disturbance around the time of 2015 Nepal earthquake. Journal of Geodesy 92, 1255-1266, 2018.
13. Kuo, C. L., Huba, J. D., Joyce, G., and Lee, L. C.: Ionosphere plasma bubbles and density variations induced by pre-earthquake rock currents and associated surface charges. Journal of Geophysical Research Atmospheres 116, -, 2011.
14. Lehtinen, N. G., and Inan, U. S.: Radiation of ELF/VLF waves by harmonically varying currents into a stratified ionosphere with application to radiation by a modulated electrojet. J. Geophys. Res. 113, 2008.
15. Lehtinen, N. G., and Inan, U. S.: Full ‐ wave modeling of transionospheric propagation of VLF waves. Geophys. Res. Lett. 36, 2009.
16. Li, Y., Zhang, L., Zhang, K., and Jin, X.: Research on the Atmospheric Electric Field Abnormality near the Ground Surface before“5. 12”Wenchuan Earthquake. Plateau and Mountain Meteorology Research 37, 49-53, 2017.
17. Liao, L., Zhao, S., and Zhang, X.: Advances in the study of transionospheric propagation of VLF waves. Chinese Journal of Space Science (in Chinese) 37, 277-283, 2017.
18. Liu, J. Y., Chen, Y. I., Chen, C. H., Liu, C. Y., Chen, C. Y., Nishihashi, M., Li, J. Z., Xia, Y. Q., Oyama, K. I., Hattori, K., and Lin, C. H.: Seismoionospheric GPS total electron content anomalies observed before the 12 May 2008 Mw7.9 Wenchuan earthquake. Journal of Geophysical Research: Space Physics 114, 2009.
19. Liu, J. Y., Chen, Y. I., Chuo, Y. J., and Tsai, H. F.: Variations of ionospheric total electron content during the Chi-Chi earthquake. Geophysical Research Letters 28, 1383-1386, 2001.
20. Liu, J. Y., Tsai, Y. B., Chen, S. W., Lee, C. P., Chen, Y. C., Yen, H. Y., Chang, W. Y., and Liu, C.: Giant ionospheric disturbances excited by the M9.3 Sumatra earthquake of 26 December 2004. Geophysical Research Letters 33, 2006.
21. Marshall, R. A., Inan, U. S., and Glukhov, V. S.: Elves and associated electron density changes due to cloud-to-gound and in-cloud lightning discharges. Journal of Geophysical Research: Space Physics 115, n/a-n/a, 2010.
22. Maurya, A. K., Venkatesham, K., Tiwari, P., Vijaykumar, K., Singh, R., Singh, A. K., and Ramesh, D. S.: The 25 April 2015 Nepal Earthquake: Investigation of precursor in VLF subionospheric signal. J Geophys Res-Space 121, 10403-10416, 2016.
23. Molchanov, O. A., Rozhnoi, A., Solovieva, M., Akentieva, O., Berthelier, J. J., Parrot, M., Lefeuvre, F., Biagi, P. F., Castellana, L., and Hayakawa, M.: Global diagnostics of the ionospheric perturbations related to the seismic activity using the VLF radio signals collected on the DEMETER satellite. Natural Hazards & Earth System Sciences 6, 745-753, 2006.
24. Namgaladze, A. A., Zolotov, O. V., and Prokhorov, B. E.: Numerical Simulation of the Variations in the Total Electron Content of the Ionosphere Observed before the Haiti Earthquake of January 12, 2010. Geomagn Aeronomy+ 53, 522-528, 2013.
25. Píša, D., Němec, F., Santolík, O., Parrot, M., and Rycroft, M.: Additional attenuation of natural VLF electromagnetic waves observed by the DEMETER spacecraft resulting from preseismic activity. Journal of Geophysical Research: Space Physics 118, 5286-5295, 2013.
26. Parrot, M., Benoist, D., Berthelier, J. J., Błęcki, J., Chapuis, Y., Colin, F., Elie, F., Fergeau, P., Lagoutte, D., and Lefeuvre, F.: The magnetic field experiment IMSC and its data processing onboard DEMETER: Scientific objectives, description and first results. Planetary & Space Science 54, 441-455, 2006.

https://doi.org/10.5194/angeo-2020-7
Preprint. Discussion started: 3 March 2020

Annales Geophysicae Discussions
Open Access
EGU

27. Parrot, M., Sauvaud, J., Berthelier, J., and Lebreton, J.: First in-situ observations of strong ionospheric perturbations generated by a powerful VLF ground-based transmitter. Geophys. Res. Lett. 34, 2007.
28. Peter, W. B., Chevalier, M. W., and Inan, U. S.: Perturbations of midlatitude subionospheric VLF signals associated with lower ionospheric disturbances during major geomagnetic storms. J Geophys Res-Space 111, 2006.
29. Pokhotelov, D., Mitchell, C. N., Spencer, P. S. J., Hairston, M. R., and Heelis, R. A.: Ionospheric storm time dynamics as seen by GPS tomography and in situ spacecraft observations. J Geophys Res-Space 113, 2008.
30. Pulinets, S. A.: Physical mechanism of the vertical electric field generation over active tectonic faults. Advances In Space Research 44, 767-773, 2009.
31. Pulinets, S. A., Boyarchuk, K. A., Hegai, V. V., Kim, V. P., and Lomonosov, A. M.: Quasielectrostatic model of atmosphere-thermosphere-ionosphere coupling. Adv. Space Res. 26, 1209-1218, 2000.
32. Shao, X., Eliasson, B., Sharma, A., Milikh, G., and Papadopoulos, K.: Attenuation of whistler waves through conversion to lower hybrid waves in the low‐altitude ionosphere. J. Geophys. Res.: Space Phys 117, 2012.
33. Shen, X., Zhima, Z., Zhao, S., Qian, G., Ye, Q., and Ruzhin, Y.: VLF radio wave anomalies associated with the 2010 Ms 7.1 Yushu earthquake. Advances in Space Research 59, 2017.
34. Shen, X. H., Zhang, X. M., Yuan, S. G., Wang, L. W., Cao, J. B., Huang, J. P., Zhu, X. H., Piergiorgio, P., and Dai, J. P.: The state-of-the-art of the China Seismo-Electromagnetic Satellite mission. Sci China Technol Sc 61, 634-642, 2018.
35. Stangl, G., Boudjada, M. Y., Biagi, P. F., Krauss, S., Maier, A., Schwingenschuh, K., Al-Haddad, E., Parrot, M., and Voller, W.: Investigation of TEC and VLF space measurements associated to L'Aquila (Italy) earthquakes. Nat Hazard Earth Sys 11, 1019-1024, 2011.
36. Starks, M., Quinn, R., Ginet, G., Albert, J., Sales, G., Reinisch, B., and Song, P.: Illumination of the plasmasphere by terrestrial very low frequency transmitters: Model validation. J. Geophys. Res.: Space Phys 113, 2008.
37. Tao, X., Bortnik, J., and Friedrich, M.: Variance of transionospheric VLF wave power absorption. J. Geophys. Res.: Space Phys 115, 2010.
38. Xu, T., Hu, Y. L., Wu, J. A., Wu, Z. S., Li, C. B., Xu, Z. W., and Suo, Y. C.: Anomalous enhancement of electric field derived from ionosonde data before the great Wenchuan earthquake. Advances In Space Research 47, 1001-1005, 2011.
39. Yao, L., Chen, H., and He, Y.: The signal to noise ratio disturbance of ionospheric VLF radio signal before the 2010 Yushu Ms7.1 earthquake. Acta Seismologica Sinica 35, 390-399, 2013.
40. Yeh, K. C., and Liu, C. H., 1972. Theory of Ionospheric Waves. Academic Press, New York.
41. Zhao, B. Q., Wang, M., Yu, T., Wan, W. X., Lei, J. H., Liu, L. B., and Ning, B. Q.: Is an unusual large enhancement of ionospheric electron density linked with the 2008 great Wenchuan earthquake? J Geophys Res-Space 113, 2008.
42. Zhao, S., Liao, L., and Zhang, X.: Trans-ionospheric VLF wave power absorption of terrestrial VLF signal. Chinese Journal of Geophysics (in Chinese) 60, 3004-3014, 2017.
43. Zhao, S., Zhang, X., Zhao, Z., Shen, X., and Chen, Z.: Temporal variations of electromagnetic responses in the ionosphere excited by the NWC communication station. Chinese Journal of Geophysics- Chinese Edition 58, 2263-2273, 2015.
44. Zhao, S., Zhou, C., Shen, X., and Zhima, Z.: Investigation of VLF transmitter signals in the ionosphere by ZH-1 observations and full-wave simulation. Journal of Geophysical Research: Space Physics 124, 4697-4709, 2019.
45. Zhou, C., Liu, Y., Zhao, S. F., Liu, J., Zhang, X. M., Huang, J. P., Shen, X. H., Ni, B. B., and Zhao, Z. Y.: An electric field penetration model for seismo-ionospheric research. Advances In Space Research 60, 2217-2232, 2017.
46. Zigman, V., Grubor, D., and Sulic, D.: D-region electron density evaluated from VLF amplitude time delay during X-ray solar flares. J Atmos Sol-Terr Phy 69, 775-792, 2007.

https://doi.org/10.5194/angeo-2020-7
Preprint. Discussion started: 3 March 2020

Annales Geophysicae Discussions
Open Access
EGU

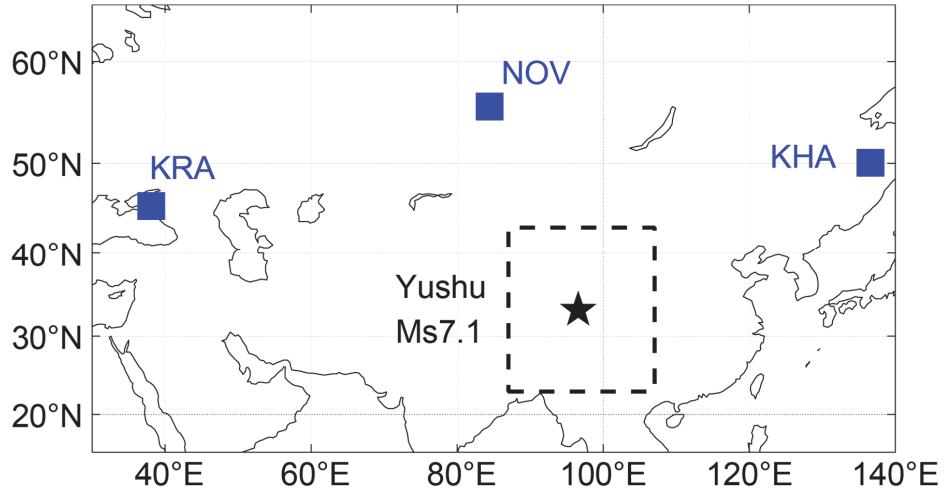

474

475 **Figure 1: The locations of transmitters and Yushu earthquake. The blue squares represent the locations of**
476 **the three transmitters (KRA, NOV, KHA) in Russia. The epicenter of Yushu earthquake is denoted by the**
477 **black star. The black square covers the region of epicenter ±10° in which the data has been studied.**

478

https://doi.org/10.5194/angeo-2020-7
Preprint. Discussion started: 3 March 2020

Annales Geophysicae Discussions
Open Access
EGU

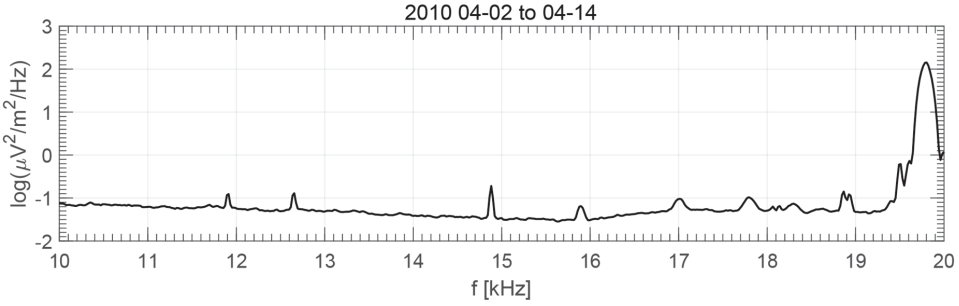

479

480 **Figure 2: The averaged electric field spectrum structure within 600 km around the epicenter of Yushu**
481 **earthquake.**

482

https://doi.org/10.5194/angeo-2020-7
Preprint. Discussion started: 3 March 2020

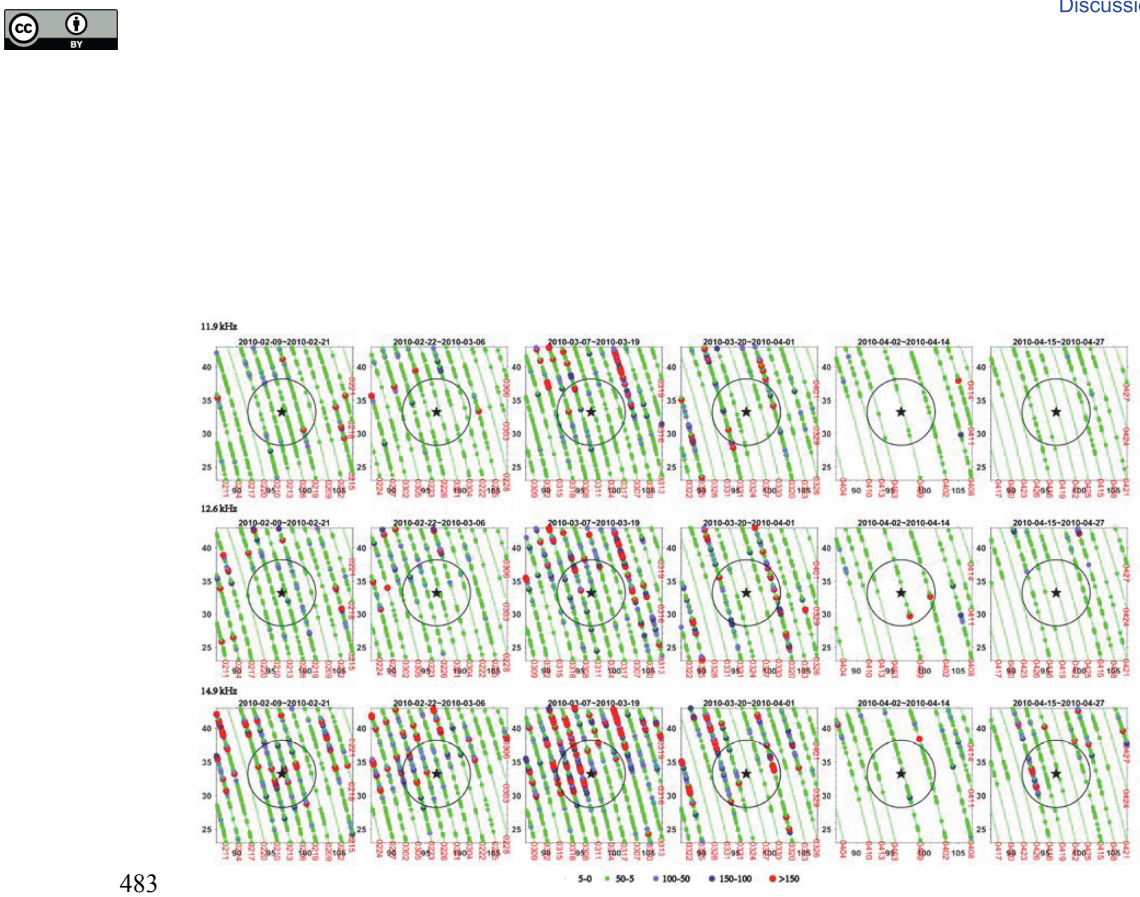

Figure 3: The evolution of SNR evolution VLF radio waves frequencies 11.9, 12.6, 14.9 kHz with Δf = 300 Hz. The black star stands for the epicenter of the Yushu earthquake, and the radius of the black circle is 600km.

https://doi.org/10.5194/angeo-2020-7
Preprint. Discussion started: 3 March 2020

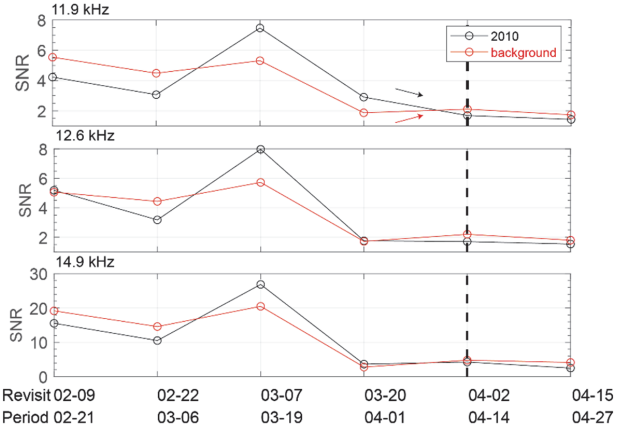

487

488 **Figure 4: The average SNR variation with revisit period inside the 600 km circle with the center of the**
489 **epicenter. The panel from top to the bottom are the SNRs at 11.9, 12.6, 14.9 kHz and the numbers of the**
490 **averaged data points. The green and red lines represent the SNR variations in 2010 and background time**
491 **separately. The black dashed line represents the period with the end date of main shock date.**

492

https://doi.org/10.5194/angeo-2020-7
Preprint. Discussion started: 3 March 2020

Annales Geophysicae Discussions
Open Access
EGU

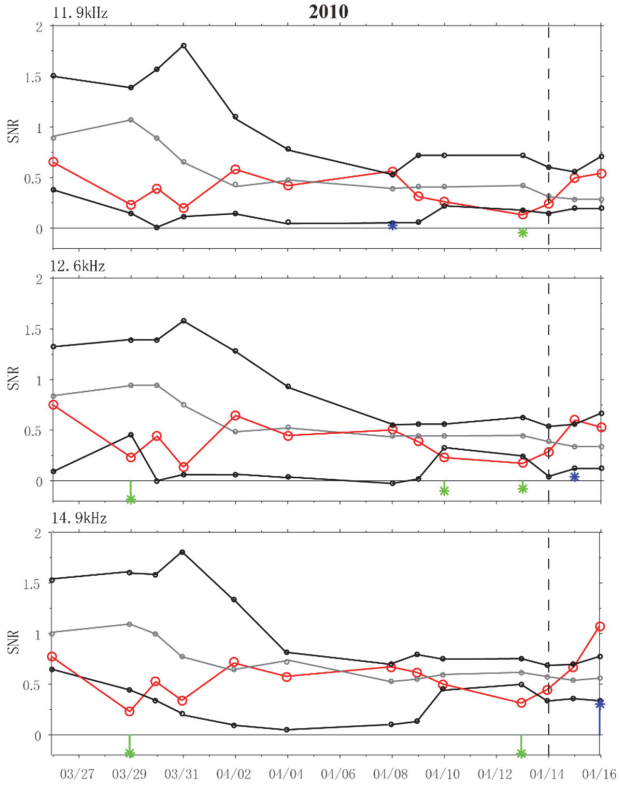

493

494 **Figure 5: A time series of SNR right above the Yushu epicenter. The Ms 7.1 Yushu earthquake occurred at**
495 **the local time 07:49:37.9 of April 14, 2010. The red, gray, and two black curves denote the observed SNR and**
496 **associated median and upper/lower bound (UB/LB), respectively. Blue and blue sgin represent the upper and**
497 **lower anomalous days identified by the computer routine, respectively. The LB and UB are constructed by**
498 **the 1–11 previous days' moving median (M), lower quartile (LQ), and upper quartile (UQ).**

499

https://doi.org/10.5194/angeo-2020-7
Preprint. Discussion started: 3 March 2020

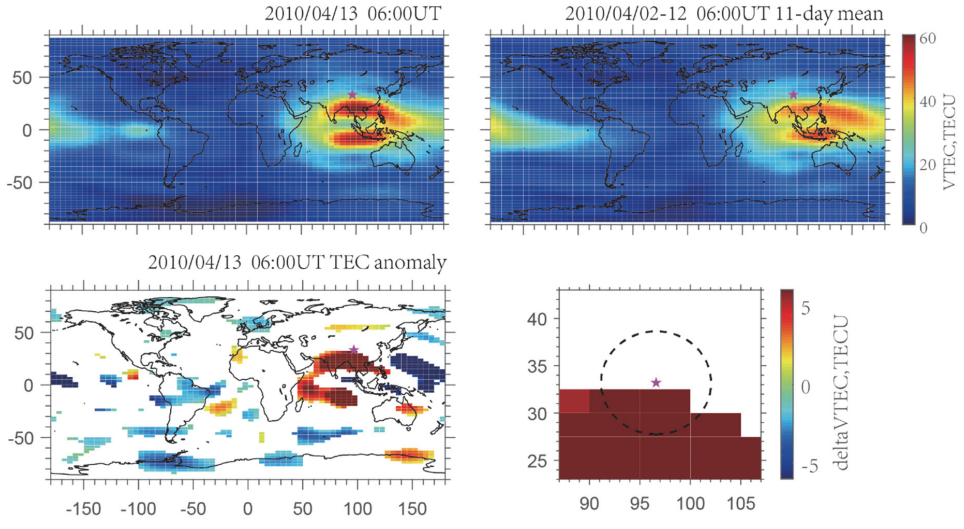

Figure 6: The spatial distribution of GPS-TEC MAP (top) and its anomalies (bottom). The GPS-TEC MAP on April 13 at UT 6:00 (left of top panel). The sliding mean of 11 days of background (right of top panel). The global anomalies in GPS-TEC MAP (left of bottom panel). The regional anomalies around epicenter of Yushu earthquake in GPS-TEC MAP (right of bottom panel). The purple pentagram indicate the epicenter and the radius of the black circle is 600km.

https://doi.org/10.5194/angeo-2020-7
Preprint. Discussion started: 3 March 2020

Annales Geophysicae Discussions
Open Access
EGU

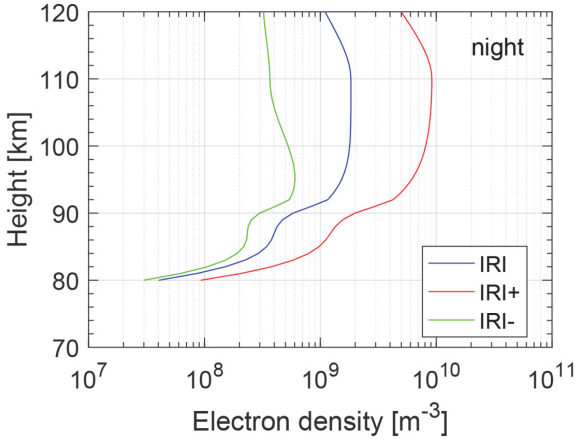

507

508 **Figure 7: The electron density profiles during night time. IRI represents the original electron density**
509 **predicted by IRI model; IRI+ represents the electron density added Gaussian shape perturbation; IRI-**
510 **represents the electron density subtracted Gaussian shape perturbation.**

511

https://doi.org/10.5194/angeo-2020-7
Preprint. Discussion started: 3 March 2020

Annales Geophysicae Discussions
Open Access
EGU

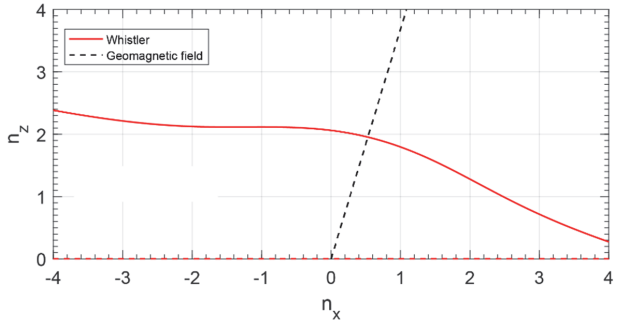

512

513 **Figure 8: The refractive index surface at 120 km. Red line shows a slice of the refractive index surface at**
514 **$n_y = 0$ of the whistler mode, calculated for $f = 11.9$ kHz at the altitude of $h = 120$ km. Black dash line**
515 **shows the direction of the geomagnetic field.**

516

https://doi.org/10.5194/angeo-2020-7
Preprint. Discussion started: 3 March 2020

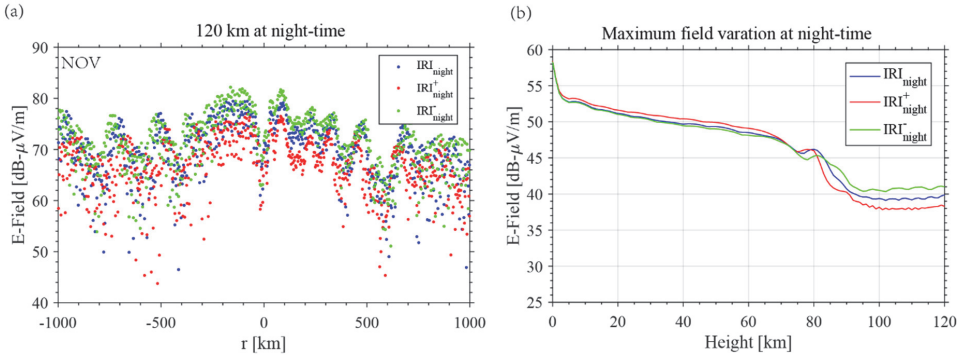

Figure 9: The total electric field excited by ground based VLF transmitter NOV with transmitting frequency f=11.9 kHz and power P=500 kW. (a) The total electric field at the altitude of 120 km in the nighttime when Gaussian shape disturbance is set at 80-120km. (b) The maximum electric field varying with altitude in the nighttime.

https://doi.org/10.5194/angeo-2020-7
Preprint. Discussion started: 3 March 2020

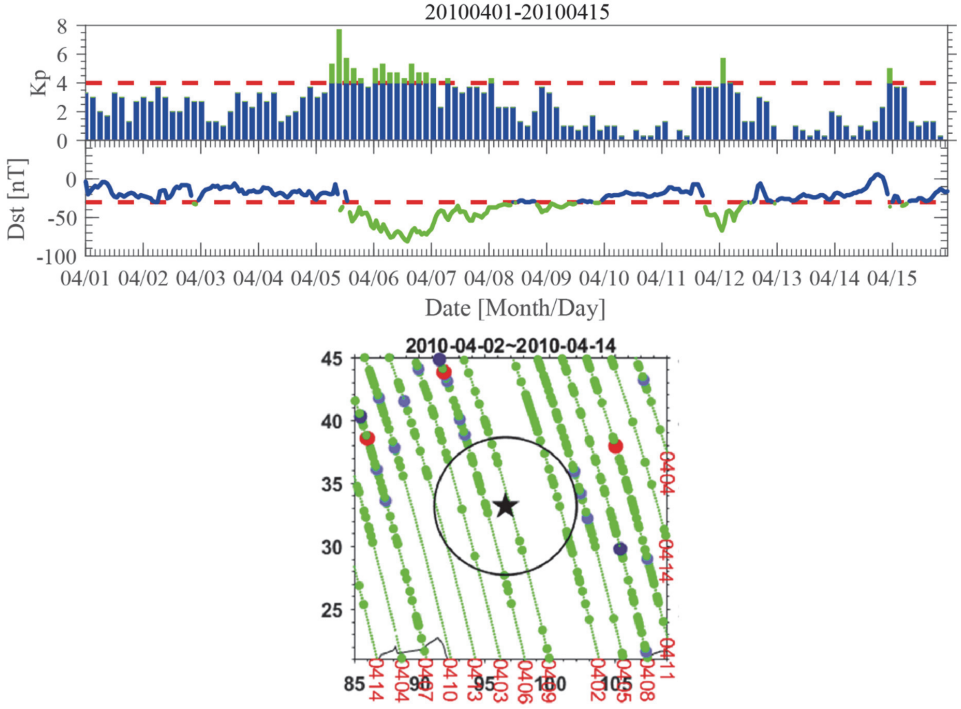

Figure 10: The Kp and Dst index in April 2010 (top panel). The SNR distribution from April 2 to April 14. (bottom panel)